J Mater Sci (2008) 43:7379–7384
DOI 10.1007/s10853-008-2788-6

ULTRAFINE-GRAINED MATERIALS

Quasi-static and dynamic mechanical properties of commercial-purity tungsten processed by ECAE at low temperatures

Z. Pan · Y. Z. Guo · S. N. Mathaudhu · L. J. Kecskes · K. T. Hartwig · Q. Wei

Received: 16 April 2008 / Accepted: 6 June 2008 / Published online: 21 July 2008

Abstract In this work, we have processed commercial purity tungsten (W) via different routes of equal-channel angular extrusion (ECAE) at temperatures as low as 600 °C. We have systematically evaluated the quasi-static and dynamic compressive behaviors of the processed W. Quasi-static compression tests were performed using an MTS hydro-servo system at room temperature. It is observed that samples ECAE processed at 800 °C show higher yield and flow stresses than those processed at other temperatures; no obvious strain hardening is observed in the quasi-static stress–strain curves. Quasi-static strain rate jump tests show that the strain rate sensitivity of ECAE W is in the range of 0.02 to 0.03, smaller than that of coarse-grained W. Uni-axial dynamic compressive tests were performed using the Kolsky bar (or split-Hopkinson pressure bar, SHPB) system. Post-loading SEM observations revealed that under dynamic compression, the competition between cracking at pre-existing extrinsic surface defects, grain boundaries, and uniform plastic deformation of the individual grains control the overall plastic deformation of the ECAE W. The existence of flow softening under dynamic loading has been established for all of the ECAE W specimens.

Z. Pan · Y. Z. Guo · Q. Wei (✉)
Department of Mechanical Engineering and Engineering Science, University of North Carolina at Charlotte, 9201 University City Boulevard, Charlotte, NC 28223-0001, USA
e-mail: qwei@uncc.edu

S. N. Mathaudhu · L. J. Kecskes
U.S.-Army Research Laboratory, Weapons and Materials Research Directorate, AMSRD-ARL-WM-MB, Aberdeen Proving Ground, Aberdeen, MD 21005-5069, USA

K. T. Hartwig
Department of Mechanical Engineering, Texas A&M University, College Station, TX 77843-3123, USA

Introduction

Tungsten (W) is a refractory body-centered cubic (BCC) metal with high mass density, melting point, and strength, which lend it to many important applications. One particular potential application is to replace depleted uranium (DU) for the fabrication of kinetic energy penetrators, which requires a self-sharpening behavior during plastic deformation under dynamic loading. In other words, shear localization in the form of shear banding should be the dominant deformation and material discarding mode at high loading rates. Unfortunately, for commercial purity tungsten, the interstitial impurities tend to segregate at the grain boundaries (GBs), which decrease the cohesion strength of GBs [1]. As a result, at ambient temperature, axial cracking turns out to be the predominant deformation and failure mode under uni-axial compressive loading of commercial purity coarse-grained (CG) W [2–4].

Many efforts have been undertaken to render W to deform by adiabatic shear localization. One possible way is to refine the grain size of CG W through two general methods: bottom-up and top-down [5]. In the first method, nanometer-sized particles synthesized via various techniques are compacted into a bulk form under high pressure at relatively high temperatures. However, this unavoidably introduces impurities into the material. Another issue with the bottom-up method is the difficulty in the control of density and grain size, since full density and nanometer grain size are difficult to achieve simultaneously [6]. On the other hand, the top-down method starts with a bulk

material with coarse grains or a single crystal and refines the grain size into the ultrafine grained (UFG, grain size <500 nm but >100 nm), and even the nanocrystalline (NC, grain size <100 nm), regime. Severe plastic deformation (SPD), including equal-channel angular extrusion (ECAE) and high pressure torsion (HPT), is a commonly used technique [7, 8]. In contrast to some bottom-up methods, this top-down technique has the advantage of cleanness: no impurities are introduced during SPD process. However, commercial purity W has been proved to be difficult to process using ECAE due to its poor workability resulting from the weak grain boundaries [5]. In order to improve the material's workability, the extrusion temperature needs to be above the ductile to brittle transition temperature (DBTT); for W, the DBTT is above 150 °C [9, 10]. Recent investigations have demonstrated that ECAE W at temperatures around 1000 °C (which is still lower than the recrystallization temperature of W (about 1250 °C [10]), plus warm rolling can reduce the grain size to about 500 nm, and intensive adiabatic shear bands were observed for the first time during high rate uni-axial compressive loading [4, 11, 12].

In this work, we have processed commercial purity W via different ECAE routes at temperatures from 600 to 1200 °C and have systematically evaluated the quasi-static and dynamic compressive properties of the processed extrudates using an MTS hydro-servo system and a Kolsky bar system (also known as a Split Hopkinson pressure bar, SHPB). Optical microscopy and scanning electron microscopy (SEM) have been used to observe the side surfaces of the samples before and after loading to understand the deformation and failure mechanisms during quasi-static and dynamic compression.

Experimental procedures

The starting material was commercial purity (metals basis) W purchased from Alfa Aesar (Ward Hill, MA) in billet form. The as-received billets were formed via the sintering and extrusion of W powder. The material was processed using ECAE at different temperatures, with various routes at a punch speed of 25 mm/s. Determined by the route [13] and temperature for the ECAE process, we obtained the following specimens: 600-2B, 800-2B, 800-4Bc, 800-4E, 1000-2B, 1000-4Bc, 1000-4E, 1200-2B, and 1200-4E, where the first part of the sample label indicates the temperature (°C) at which ECAE was performed and the second part identifies the number of passes for a specific ECAE route. For example, 600-2B means the tungsten billet was ECAE processed through two passes using route B at 600 °C. Several specimens were cut from the as-processed billets using wire electrical discharge machining (EDM) for the quasi-static and dynamic test. Specimen dimensions for the quasi-static test using the MTS 810 hydro-servo system were $\sim 2.5 \times 2.5 \times 5.0$ mm (with square cross section); specimen dimensions for dynamic test using Kolsky bar were $\sim 2.5 \times 2.5 \times 2.0$ mm (the square faces are the loading faces). Loading is applied in the extrusion direction of the specimens. The strain rates for quasi-static and dynamic test were 10^{-4} and 3000–4000 s^{-1}, respectively. Details of Kolsky bar technique can be found in [14]. Quasi-static strain rate jump tests were also performed to evaluate the strain rate sensitivity of the specimens. Lubricants were applied on the specimen loading faces to reduce or eliminate friction. Before mechanical loading, two adjacent sides of each specimen were polished to a mirror finish for before- and post-loading examinations using optical microscopy and SEM.

Results and discussion

Figure 1 shows the average grain size of the nine ECAE processed W billets. The minimum grain size is 0.332 μm, achieved by ECAE through four passes using route 4E at 800 °C. It is shown that the average grain size decreases with decreasing ECAE temperature when other conditions remain the same. However, further lowering of ECAE temperature may not benefit grain size reduction due to the limited number of passes that can be applied, as the grain size of the specimen 600-2B is 0.397 μm. Mechanical testing to be presented later demonstrates that this sample also exhibits the lowest apparent yield and flow stress, with some serrated flow behavior. This is presumably due to the exacerbated cracking during low temperature ECAE, as cracking might have diminished the actual plastic strain that contributed to grain size refining. Furthermore, route E at 800 °C appears to have the best grain size refining effect among all the routes.

Figure 2a displays the optical images of the side faces of the as-received samples prior to mechanical testing; Figures 2b and c are scanning electron microscopic images of ECAE processed samples before mechanical testing with

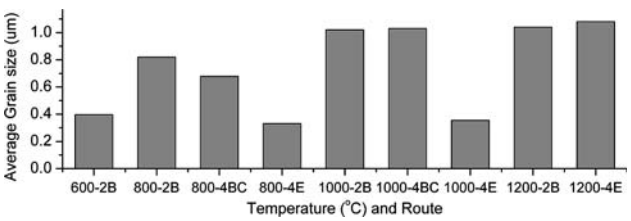

Fig. 1 Average grain size of nine ECAE processed W. The minimum grain size is 0.332 μm, corresponding to a billet ECAE processed through four passes using route E at 800 °C (800-4E in the plot). Please see text for labeling scheme

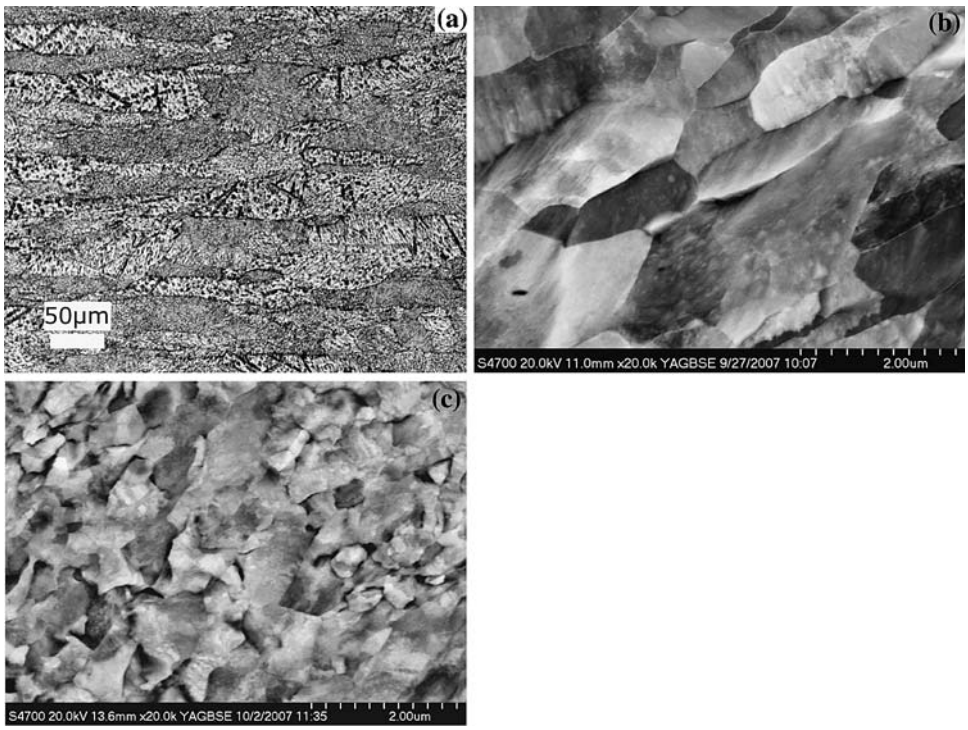

Fig. 2 Optical image of side-faces of as-purchased (**a**) and scanning electron microscopic images of ECAE processed (**b**) 1000 °C-2B, average grain size ~1000 nm; (**c**) 1000 °C-4E, average grain size ~400 nm) samples before mechanical loading. The as-purchased W was polished followed by chemical etching using standard Murakami solution to reveal the microstructure. The ECAE processed samples were polished but not etched. Loading direction will be very close to the extrusion direction for the ECAE-processed samples

SEM images taken in the high-resolution backscatter mode. The loading direction will be along a direction parallel to the vertical. Elongated grains with sizes of ~50 to 100 μm can be observed in the as-received (extruded) sample (Fig. 2a); grain size of ~1000 nm is observed in the 1000-2B material (Fig. 2b, also Fig. 1); grain size of ~400 nm is observed in the 1000-4E sample (Fig. 2c, also Fig. 1). Results in Figs. 1 and 2 indicate that above 1200 °C, due to dynamic recrystallization and grain growth, ECAE is not quite efficient in refining the grain size of commercial purity W after initial grain size refinement from the first pass.

Figure 3 shows the quasi-static (a) and dynamic (b) true stress–true strain curves of the ECAE-processed and the as-received W. From the quasi-static stress–strain curves, it can be seen that most of the processed samples show an almost elastic-perfectly plastic behavior with only slight strain hardening. However, this is not the case for specimens 1000-2B and 600-2B, where both show a strain softening behavior and have flow stresses lower than that of the as-received W, although the average grain size is far less than that of the latter. This phenomenon obviously contradicts the Hall-Petch relation that the yield stress increases with decreasing grain size of metals [15, 16]. This observation indicates the contribution of some different deformation mechanisms, which will be discussed in further detail later. The as-received W shows the strongest strain hardening behavior compared with all the processed samples. A slight stress drop after yielding can also be observed, which might come from the weak GBs of this commercial purity tungsten. The absence of this apparent stress drop in the ECAE processed specimens may suggest that the ECAE processing has somehow strengthened some of the GBs of the original W. From the quasi-static stress–strain curves, we can also observe that specimen 800-4E shows the maximum flow stress, agreeing with the minimum grain size shown in Fig. 1, whereas specimen 600-2B has the lowest flow stress, and it also exhibits a serrated flow behavior in the stress–strain curve. This result is at odds with the grain size of 600-2B (~400 nm), which is the smallest compared to the rest of the ECAE-processed specimens and the as-received material and should therefore exhibit the highest flow stress according to the Hall-Petch effect. We envisage that such behavior might be a consequence of ECAE-induced micro-cracks in the specimen, as the ECAE processing temperature for this sample is lower compared to other specimens. Likewise, ECAE-induced cracks could also explain the serrated flow behavior of sample 600-2B.

Different from the quasi-static stress–strain curves, the dynamic stress–strain curves of all the ECAE specimens show flow softening. In comparison, the as-received control sample exhibits some strain hardening at small strains under dynamic loading; the dynamic stress–strain curve then levels off, presumably due to adiabatic heating.

One important parameter that characterizes plastic deformation of metals is the strain-rate dependence. This is particularly the case where plastic instability is of great

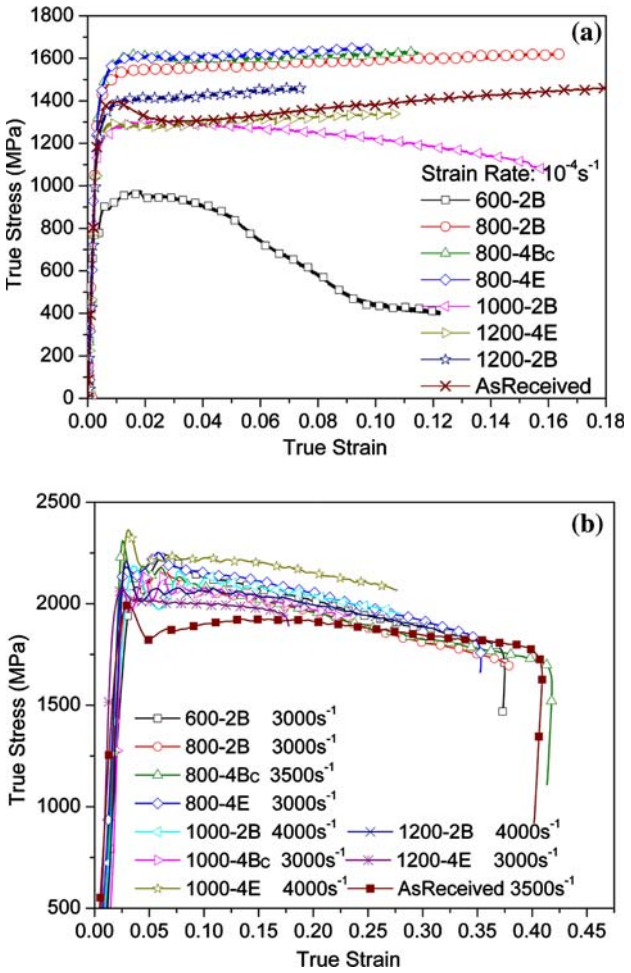

Fig. 3 The quasi-static (**a**) and dynamic (**b**) true-stress–true-strain curves of the ECAE-processed and the as-received W samples. The insets define the ECAE conditions and strain rates

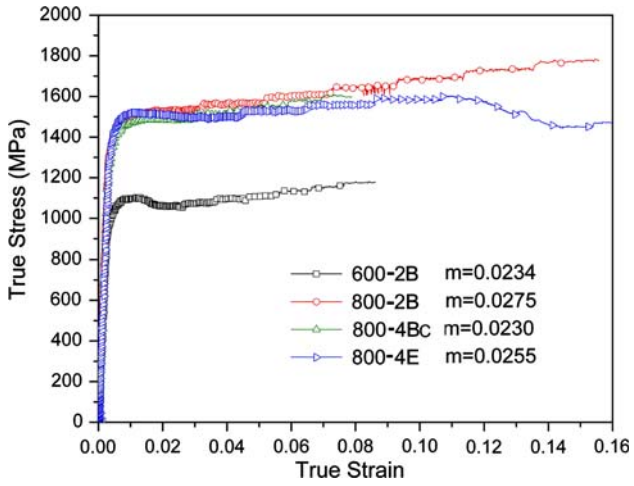

Fig. 4 The true stress–true-strain curves showing the results of the strain-rate jump experiments of some of the ECAE-processed specimens. The derived strain rate sensitivity values are also given in the plot

concern [17, 18]. There are a number of ways to measure the strain-rate dependence of a material's mechanical behavior. In this work, we used the strain-rate jump test, where during uniform plastic deformation, the cross-head speed is abruptly increased, leading to a sudden jump in the imposed strain rate. Figure 4 displays the true-stress true-strain curve for the strain-rate jump tests of a few ECAE processed specimens. Usually, power law dependence in the form $\sigma/\sigma_0 = (\dot{\varepsilon}/\dot{\varepsilon}_0)^m$ is assumed to represent the strain rate dependence of a material. In this equation, σ is the flow stress at a given strain, σ_0 is a normalizing stress, $\dot{\varepsilon}$ is the imposed strain rate, and $\dot{\varepsilon}_0$ is a normalizing strain rate. The parameter m is usually called the strain rate sensitivity (SRS) of a material under mechanical testing. Using this approach, we derive an SRS value in the range of 0.02 to 0.03 for the ECAE-processed commercial purity W. This SRS range is in accordance with that of rolled- and SPD-processed W [4, 12, 17, 19], and is smaller than that of the SRS of coarse-grained (CG) W ($\sim$0.042 [9]). Similar to Fig. 3, the flow stress of specimen 600-2B is lowest among all the tested specimens although its SRS does not differ much from those of other specimens.

Figure 5 displays images of the polished side surface of the as-received W after dynamic loading. Some cracks are observed in Fig. 5a. The majority of cracks are along the loading direction (axial cracks), typical of CG W and other brittle materials [2, 3]. The image shown in Fig. 5b is taken at a higher magnification from one corner of another side-face of the same sample tested. No obvious localized shear or flow like deformation can be observed in this specimen, even though some cracks are in or near the maximum shear stress direction.

Figure 6 shows the SEM images of the corners of the post-loading side faces of specimens 1000-4Bc and 800-2B. Different orientations and distributions of cracks can be observed here. It should be pointed out that the apparent axial cracks are caused most probably by the oxide layer introduced during electrical discharge machining, which was not completely removed during subsequent sample preparation. Such surface cracks are not expected to extend deep into the specimen, neither do they affect the overall stress–strain behavior of the specimen. For specimen 1000-4Bc, most of the cracks distribute along the maximum shear stress direction, with a superimposed localized shearing mode, which might appear more obvious if the EDM oxide layer had been removed completely. Specimen 800-2B show a similar flow and cracks mode; the deformation is less heterogeneous, and perhaps more adiabatic in nature. This may provide an explanation for the observed flow softening in the dynamic stress–strain curves for the 800-2B specimen, shown in Fig. 3. Figure 7 shows the SEM images of the post-loading side-faces of the 1200-

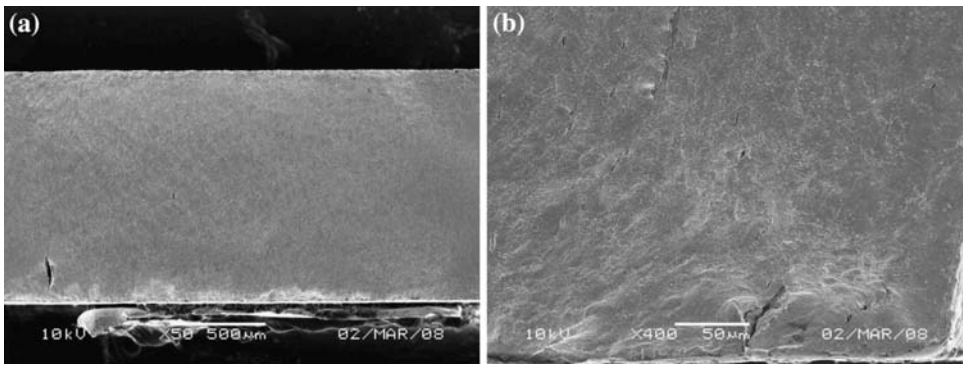

Fig. 5 SEM images of side-faces of the as-received W after dynamic loading. (**a**) Low magnification image. (**b**) Higher magnification image of the same specimen. Loading direction is vertical. Features typical of post-loading surfaces of brittle materials are shown, viz. cracks in the direction of loading

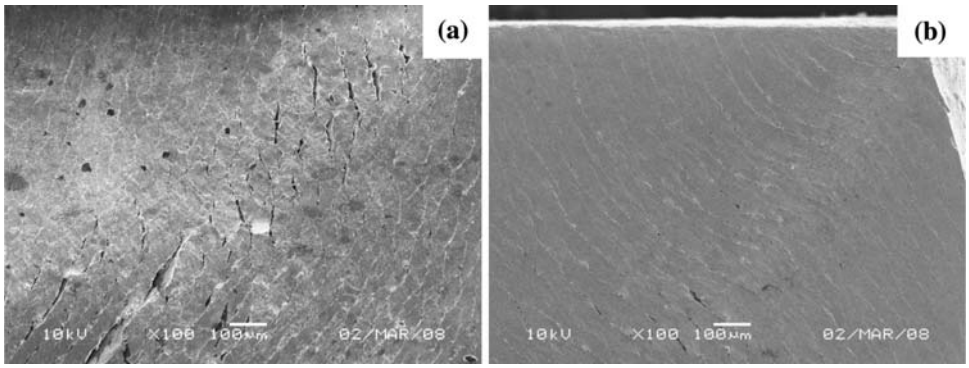

Fig. 6 Post-loading SEM images of the side-faces of specimens 1000-4Bc (**a**) and 800-2B (**b**). It is noted that the majority of cracks are oriented along the maximum shear stress direction. Note that most cracks in (**a**) and some cracks in (**b**) are those of the surface oxide layer introduced by electrical discharge machining. Evidence of adiabatic shear localization can be established. Loading is vertical (close to the extrusion direction)

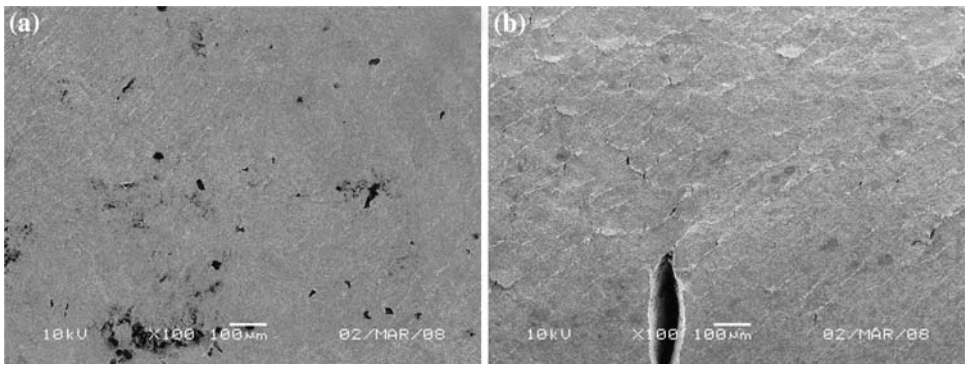

Fig. 7 Post-loading SEM images of side-faces of specimens 1200-4E (**a**) and 1000-4E (**b**). Loading is vertical. The primary features of the 1200-4E specimen are not much different from those of the as-received material

4E and 1000-4E specimens. In sample 1200-4E, parallel cracks are present at an angle of $\sim 45^{o}$ with respect to the loading direction. There are also some cracks running in the loading direction, making it not much different from the as-received material. In specimen 1000-4E, the cracks are more apparent. These two samples show no strong localized shear deformation compared to Fig. 6, thus giving the weakest flow softening among all the ECAE-processed specimens, as was shown in Fig. 3.

In summary, in the ECAE-processed commercial purity W, some evidence was established for adiabatic shear localization under uni-axial dynamic loading. However, to further enhance the propensity for adiabatic shear localization, cracking should be avoided, as the overall deformation is a competition between cracking along the pre-existing weak links such as the weak grain boundaries and uniform deformation leading to adiabatic temperature rise. Further elaboration should be undertaken to optimize the ECAE process for products with improved GB strength, enhanced ductility, and exhausted strain hardening capacity.

Previously, it has been shown that strong adiabatic shear localization occurs in the ECAE + warm-rolling and high pressure torsion (HTP) processed W under dynamic

compressive loading, where no cracks were observed during dynamic deformation, except the subsequent cracks following the shear localization [4, 11, 12]. However, as has been described in this work, W specimens processed by ECAE alone exhibit cracks upon dynamic loading of specimens, even though evidence of localized shearing was also observed. This is probably because rolling or HPT processes might have altered the prior texture or grain structure, and as a consequence, helped to heal pre-existing inter-granular cracks or hairline cracks generated during ECAE process. Recall that the measured strain rate sensitivity of ECAE processed tungsten was determined to be about 0.025 in this work, which is almost the same as the SRS value of ECAE + warm-rolling processed W. It should be obvious that healing of the cracks and simultaneous exhaustion of the strain hardening capacity of the W is the primary objectives for future efforts in lieu of the desired applications.

Summary and concluding remarks

After extruding commercial purity W by ECAE at different processing temperatures and using various extrusion routes, we have obtained a number of processed samples with average grain sizes ranging from 300 nm to 1.0 μm. Mechanical testing under quasi-static and dynamic loading showed that the ECAE-processed W exhibits reduced strain hardening compared to the unprocessed, as-received sample. The strain rate sensitivity of the ECAE W has been reduced to $\sim$0.025, almost the same value as that of ECAE + warm-rolled W, and significantly smaller than that of CG W. Analysis of mechanical testing results and SEM observations of the post-loading side-faces suggests that the deformation mode of ECAE-processed W is a competition between cracking along weak GBs, ECAE-induced cracks, and uniform crystal plasticity. Certain diffuse plastic localization is observed under dynamic compression, which explains the dynamic flow softening in the dynamic stress–strain curves. Decreasing the ECAE temperature helps to generate finer grains, but causes it to be more susceptible to inter-granular fracture. Optimization of the ECAE process in terms of the processing temperatures, number of passes, and type of route will be considered in the future.

Acknowledgements This work has been supported by the U.S. Army Research Laboratory under contract # W911QX-06-C-0124. The authors would like to thank Ms. Xueran Liu (University of North Carolina at Charlotte) for assistance with SEM operations.

References

1. Krasko GL (1993–1994) Int J Refract Met Hard Mater 12:251
2. Dummer T, Lasalvia JC, Ravichandran G, Meyers MA (1998) Acta Mater 46:6267. doi:10.1016/S1359-6454(98)00255-9
3. Lennon AM, Ramesh KT (2000) Mater Sci Eng A 276:9. doi:10.1016/S0921-5093(99)00517-1
4. Wei Q, Jiao T, Ramesh KT, Ma E, Kecskes LJ, Magness L et al (2006) Acta Mater 54:77. doi:10.1016/j.actamat.2005.08.031
5. Kecskes LJ, Cho KC, Dowding RJ, Schuster BE, Valiev RZ, Wei Q (2007) Mater Sci Eng A 467:33. doi:10.1016/j.msea.2007.02.099
6. Lu K (2008) Int Mater Rev 53:21. doi:10.1179/174328008X254358
7. Valiev RZ, Estrin Y, Horita Z, Langdon TG, Zehetbauer M, Zhu YT (2006) JOM-US 58:33
8. Wei Q, Ramesh KT, Kecskes LJ, Mathaudhu SN, Hartwig KT (2008) Mater Sci Forum 579:75
9. Bechtold JH (1956) J Met Trans AIME 206:142
10. Farrell K, Schaffhauser AC, Stiegler JO (1967) J Less Common Met 13:141. doi:10.1016/0022-5088(67)90177-4
11. Wei Q, Zhang H, Schuster BE, Ramesh KT, Valiev RZ, Kecskes LJ et al (2006) Acta Mater 54:4079. doi:10.1016/j.actamat.2006.05.005
12. Wei Q, Ramesh KT, Ma E, Kesckes LJ, Dowding RJ, Kazykhanov VU et al (2005) Appl Phys Lett 86:101907. doi:10.1063/1.1875754
13. Barber RE, Dudo T, Yasskin PB, Hartwig KT (2004) Scripta Mater 51:373. doi:10.1016/j.scriptamat.2004.05.022
14. Follansbee PS (1985) In ASM metals handbook. American Society of Metals. p 190
15. Hall EO (1951) P Phys Soc B 64:747
16. Petch NJ (1953) J Iron Steel I 174:25
17. Wei Q (2007) J Mater Sci 42:1709. doi:10.1007/s10853-006-0700-9
18. Wei Q, Cheng S, Ramesh KT, Ma E (2004) Mater Sci Eng A 381:71. doi:10.1016/j.msea.2004.03.064
19. Wei Q, Kecskes LJ (2008) Mater Sci Eng A. doi:10.1016/j.msea.2008.01.013